Journal of Materials Chemistry B

Accepted Manuscript

ROYAL SOCIETY OF CHEMISTRY

www.rsc.org/materialsB

Hierarchical, stretchable and stiff fibrous biotemplate engineered using stagger-electrospinning for augmentation of rotator cuff tendon-healing

Song Zhao[a,c1], Xin Zhao[d1], Shikui Dong[c1], Jia Yu[a,b], Guoqing Pan[a,b], Yang Zhang[c], Jinzhong Zhao[c*], Wenguo Cui [a,b,d*]

[a] Orthopedic Institute, Soochow University, 708 Renmin Rd, Suzhou, Jiangsu 215006, P.R. China.

[b] Department of Orthopedics, The First Affiliated Hospital of Soochow University, 188 Shizi St, Suzhou, Jiangsu 215006, P.R. China

[c] Department of Arthroscopic Surgery, Shanghai Sixth People's Hospital, Shanghai Jiao Tong University, School of Medicine, 600 Yishan Road, Shanghai, 200233, P.R. China

[d] Center for Biomedical Engineering, Department of Medicine, Brigham and Women's Hospital, Harvard Medical School, Cambridge, MA, 02139, USA.

[1] These authors contributed equally to this work.

* Corresponding author:

W Cui, *E-mail:* wgcui80@hotmail.com; Tel. (Fax): (+86) 512-6778-1420.

J Zhao, *E-mail:* zhaojinzhongdoctor@163.com; Tel: (+86) 21-6436-9181-5809; Fax: (+86)21-6470-1361.

Abstract

Regeneration of fibrocartilage at the tendon-bone insertion site in rotator cuff tears (RCTs) is challenging due to the complexity of its composition and mechanical properties. In this study, hierarchical, stretchable and stiff fibrous scaffolds composed of microfibers of poly (ε-caprolactone) (PCL) and nanofibers of chitosan (CS) were fabricated using stagger-electrospinning for augmentation of RCT-healing. It was found that the composite PCL-CS scaffolds had significantly improved strength and failure strain compared to the control CS scaffolds and increased stiffness compared to the control PCL scaffolds. These scaffolds also showed enhanced hydrophilicity, water absorption and faster degradation rate compared to the PCL scaffolds. They, additionally, demonstrated better fibroblast attachment and proliferation compared to the PCL scaffolds. Radiological and histological analysis revealed that the PCL-CS scaffolds enhanced new bone formation (mineralization), collagen and glycosaminoglycan expression (major components of extracellular matrix) compared to the PCL scaffolds. Furthermore, the torn tissues at the tendon-bone insertion site regenerated with the PCL-CS scaffolds showed higher strength and failure strain as well as stiffness compared to those repaired using the PCL scaffolds. The above results have suggested that the hierarchical, stretchable and stiff fibrous scaffolds engineered using stagger-electrospinning boast great potential for augmentation of RCT-healing.

Keywords: Rotator cuff tear, stagger-electrospinning, micro and nano-fibers, poly (ε-caprolactone), chitosan.

1. Introduction

Rotator cuff tear (RCT) is a common disease in the elderly, which may lead to shoulder pain and disability.[1,2] RCT often occurs at the tendon-bone insertion site (TBS).[3] TBS is a fibrocartilaginous transition zone between tendon and bone, which serves to minimize stress concentration at the junction between soft tissue (tendon) and hard tissue (bone) and to support the communication among multiple cell types to maintain interface function and homeostasis.[4]

In order to regenerate this multi-tissue transition and aid RCT healing, various methods have been used including the reinforcement of tendon-to-bone fixation,[5] application of growth factors,[6,7] administration of bone-marrow derived mesenchymal stem cells,[8] and use of low-intensity pulsed ultrasound treatment.[9] However, these methods generally cannot result in the production of normal, healthy tissue at the insertion site due to either lack of proper mechanical reinforcement or biological signals[10] and thus repair of RCT usually suffers from high failure rate.[3,11,12] Thus, development of scaffolds to support flexible fibrocartilage regeneration at TBS has become an attractive strategy for augmentation of RCT healing.

As native tendon-to-bone tissues serve as attachment of tendon (soft tissue) to bone (hard tissue) and exhibit typical 'soft tissue' behavior - capable of withstanding tension and 'hard tissue' behavior -able to resist force,[13,14] ideally, the scaffolds for functional and integrative TBS repair needs to 1) be stretchable to allow connection and movement between bone and tendon as well as stiff to provide mechanical support for both tendon and bone tissue and 2) be biocompatible as well as mimic the ultrastructural organization of native tissue to allow better fibrocartilage regeneration.

Electrospinning is a robust scaffold fabrication technique that can generate fibrous scaffolds of different chemical and physical properties via using different polymers. Dual-scale fibrous scaffolds have been developed by electrospinning. Previous studies

have found that microfibers of poly (ε-caprolactone) (PCL) or startch/PCL demonstrated improved cell viability, spreading and proliferation after incorporating its nanoscale counterparts.[15-17]. Additionally, incorporation of collagen nanofibers to PCL microfibers have shown similar results due to the nanotopography in the scaffold, chemical composition by use of a functional biocomposite, and an enlarged inner surface of the structure for cell attachment and growth.[18] Moreover, the dual-scale fibrous scaffolds had superior mechanical properties in comparison with the controls (micro- or nanofibers alone).[17] These dual-scale electrospun fibrous scaffolds are thus considered as promising candidates to repair tendon-to-bone junctions.[19-21] However, current reports focus mainly on the cellular response to the dual-scale fibers but fail to match the material bio-mechanics and micro/nano-structure to the tendon-bone insertion site. Therefore, the aim of this project was to fabricate scaffolds which were of comparable modulus to the tendon-bone insertion site and of similar nanostructure to the native tissue for cell proliferation and tissue regeneration.

In particular for our purposes, PCL microfibers and chitosan (CS) nanofibers were stagger-electrospun to fabricate the scaffolds. According to literature, electrospining PCL has resulted in biocompatible scaffolds with high mechanical flexibility which may be suitable for engineering tendon tissues.[22,23] CS has been widely regarded as one of the most attractive natural biopolymers for bone tissue engineering owing to its structural similarity to the glucoseaminoglycan found in bone, biocompatibility, biodegradability and high stiffness.[24,25] It is worth noticing that fibers of dual scale were used in this study as microfibrous scaffolds usually serve as good mechanical template whereas nanofibrous scaffolds are believed to better facilitate cell proliferation, extracellular matrix (ECM) deposition and tissue regeneration as the nanoscale features more closely resemble native structures of the ECM.[26,27] The reason of matching PCL with microfibers and CS with nanofibers lied in that electrospun PCL scaffolds，of more comparable mechanical properties to tendon, will serve as the mechanical template whereas CS fibers, more similar to bone chemically,

will provide the nano features to aid bone regeneration. These two types of fibers were stagger-electrospun (electrospinning individual fibers at the same time onto a rotating mandrel) to produce the composite scaffolds as this strategy was able to maintain the properties of individual fibers, contributing to the overall properties of the scaffolds in a tailored and controlled way.[28]

It is hypothesized that these materials could be combined using stagger-electrospinning to create a well-integrated dual scaffolding system that exhibits distinct mechanical properties and micro/nano structure to mimic native tissue for augmentation of RCT healing (Scheme 1). To test this hypothesis, we used a stagger-electrospinning method to spin individual PCL or CS fibers simultaneously onto a rotating mandrel to fabricate the continuous and knitted scaffolds. The ultrastructure of the scaffolds was evaluated using scanning electron microscopy (SEM). The physical properties (mechanical properties, hydrophobicity and degradation) of the scaffolds were assessed using uniaxial tensile tests, water contact angle (WAC) and gravimetric measurement, respectively. Biocompatibility of the scaffolds was assessed using *in vitro* and *in vivo* assays of cell proliferation and repair outcomes of chronic RCTs.

2. Materials and methods

2.1 Materials

Poly (ε-caprolactone) (PCL) (50 kDa, Mw/Mn=1.6) was prepared by bulk ring-opening polymerization (Jinan Daigang Co., Jinan, China). CS (85% deacetylated), trifluoroacetic acid (TFA), α-Cyclodextrin (suitable for cell culture, ≥98%) and glutaraldehyde (25 wt%) were from Sigma Aldrich, St Louis, USA. Dichloromethane and ethanol were from Chinese Medicine Group, Chemical Reagent Corporation (AR). Dulbecco's Modified Eagle Medium (DMEM) was from GIBCO, Grand Island, NY, USA, fetal bovine serum (FBS) from Hyclone, Tauranga, New Zealand and penicillin, streptomycin from Hyclone, Logan, UT, USA.

2.2 Fabrication of dual scaffolding system

The electrospinning equipment had a high voltage statitron (Tianjing High Voltage Power Supply Co., Tianjing, China), set at 10-25 kV. The electrospinning solution was added in a 5 ml syringe attached to a metal needle with 0.6 mm diameter and was electrospun at the flow rate of 0.2-6 ml/h controlled by a microinject pump (Lange Medical Instrument Co., Baoding, Hebei, China). For the PCL electrospun fibrous scaffolds, a 16.5% PCL solution in dichloromethane and ethanol (v/v, 3/1) was prepared, and PCL microfibers were fabricated using a rotating metal rod at a flow rate of 0.8 ml/h. For the CS electrospinning solution, CS was dissolved in 7 wt% TFA for 24 h at room temperature. Dual scaffolding system containing microfibers of PCL and nanofibers of CS were stagger-electrospun using a dual electrospinning process with a rotating metal drum (Φ = 10 cm) at a speed of 100 rpm, and the weight of PCL and CS is 1g and 0.3g through controlling electrospinning time. The resultant PCL-CS scaffolds were then crosslinked with 5% glutaraldehyde in ethanol solution for 20 min, followed by rinsing with large amounts of distilled water to remove excess glutaraldehyde. All of the fibrous scaffolds were lyophilized overnight to remove any solvent and water residues and stored at 4°C in a desiccator until further use.

2.3 Physical characterization of stagger-electrospun fibrous scaffolds

The thickness and size of the fibrous scaffolds were measured with a micrometer, and their density and porosity were calculated according to literature.[29] Morphology of the scaffolds was observed using SEM (FEI Quanta 200, Eindhoven, Netherlands) and the fiber diameter of the scaffolds was measured with Photoshop using the SEM images (n=20).[30]

Scaffolds (2 cm length, 1 cm width and 200 μm thickness) were stretched at a rate of 1 mm/min using an Instron 5542 mechanical tester. The tensile modulus was determined as the slope of the linear region of stress-strain curve corresponding with

0 – 5% strain. Cyclic testing was also performed on the scaffolds of the same specimen size. The specimens underwent 50 cycles at 1 mm/min between 0% and 5% strains.

The elastic region of the stress-strain curve of the scaffolds was then analyzed using finite element analysis. The finite element package ABAQUS v6.11 (Simulia, Dassault Systems, USA) was used to create the finite element mesh and implicit solver was used for the stress-strain distribution analysis.[31] The setting parameters were as follow: 1) 0.5 N tensile force were applied at all rectangle lines for the scaffolds; 2) the materials were homogeneous; 3) simplified two-dimensional shell model plane was applicable; 4) grid was the shell element (S4); 5) mesh density was calculated to verify elected 0.5 mm × 0.5 mm.

The WCAs of different fibrous scaffolds were measured using a Kruss GmbH DSA 100 Mk 2 goniometer (Hamburg, Germany, n=5). Water absorption was determined by weighing the composites before and after immersion in distilled water for 12 h. Excess water was removed from the samples by gently blotting with filter paper prior to the second weighing. The degradation evaluations were performed as described by Zhu *et al.*[17]

2.4 *In vitro* cell culture on scaffolds

$C_3H_{10}T_{1/2}$ mouse fibroblasts (C_3) were used to evaluate cell proliferation on different electrospun fibrous scaffolds. The cells were cultured in DMEM supplemented with 10% FBS and antibiotics (penicillin 100 U/ml, streptomycin 100 g/ml) at 37°C. After sterilization via immersion in 75% ethanol for 1.5 h in a 24-well plate, the specimens were washed repeatedly with phosphate buffered saline (PBS) to remove residual ethanol. Cells were then seeded directly onto the specimens at a density of 4×10^4 cells /cm^2 (for adhesion study) or 3×10^3 cells /cm^2 (for proliferation study) and incubated for further study on day 1, 3 and 7.

The cell morphology on different scaffolds were observed using SEM (FEI Quanta 200, The Netherlands) after fixation with 2.5% glutaraldehyde and following dehydration through a graded ethanol series. Cell proliferation on different specimens was tested using MTT assay (Sigma, St Louis, MO, USA) according to manufacturer's instruction and absorbance at 490 nm was determined using a spectrophotometer (Synergy 2; BioTek, Winooski, VT).

2.5 *In vivo tissue regeneration using c*hronic RCT model

144 male Sprague-Dawley rats weighing between 350 and 400 g were used in this study. Surgical procedures were performed according to previously published studies.[32,33] Briefly, first, to create a chronic RCT model, the left shoulder of the rats were surgically injured (i.e., detachment of the left supraspinatus tendon from its insertion site on the humerus) and healed for three weeks. During the three weeks of healing, the rats received oral metamizole and subcutaneous buprenorphine every 12 h for the first three days after the surgery. After three weeks of healing, the rats were randomized into three groups for secondary repair surgery. In the control group, the tendon was reattached to its original anatomic footprint (transosseous repair) (n=48). In the experimental groups, 96 rats underwent transosseous repair and were implanted with either pure PCL scaffolds (n=48) or PCL-CS scaffolds (n = 48) to augment the repair. The subsequent wound closure and post-operative treatment was evaluated using radiological, histologic and biomechanical investigations.

2.5.1 Microcomputed tomography analysis

At 2, 4 and 8 weeks after surgery, 24 animals (8 animals per group per time period) were allocated for microcomputed tomography (microCT) analysis. After necropsy, each shoulder girdle (including only the supraspinatus tendon-bone complex and the proximal third of the humerus) was fixed in 10% neutral buffered formalin. With micro-CT (eXplore Locus SP; GE Healthcare, London, Ontario, Canada), the bone

density and new bone formation were assessed at the tendon insertion site on the greater tuberosity. Each sample was scanned using the conditions of 80 kV, 450 μA and a 0.045 mm effective pixel size. With a global threshold for each specimen, the images were thresholded to distinguish bone voxels. Three-dimensional (3D) reconstructed images were obtained after thresholded scan, with a customized 4 mm × 4 mm cylindrical region of interest (ROI). The ROI was centered at the surface of the repaired supraspinatus tendon-bone insertion site which contained the distal portion of the supraspinatus tendon and the bony footprint.[34,35] The bone mineral density (BMD), tissue mineral density (TMD), and bone volume fraction (bone volume/total volume, BV/TV) were calculated for a volume of interest at the greater tuberosity.

2.5.2 Histomorphometric analysis

After microCT analysis, the tissue specimens were decalcified with Immunocal (Decal, Congers, New York) and embedded in paraffin. 5 μm thick sections were cut through the repaired supraspinatus tendon and the greater tuberosity in the coronal plane. The tissue sections were stained with hematoxylin and eosin, safranin O/fast green and picrosirius red, respectively.

H & E staining was used to examine the scaffold integration with adjacent host tissue. The tissue sections stained with safranin O/fast green were analyzed to determine the total area of new fibrocartilage formation at the insertion site of the rotator cuff repair using light microscopy (Leica DM4000B, Leica, Solms). Digital images of the stained tissue sections were taken using a Leica DFC420C camera (Leica, Solms). Image J software (National Institutes of Health, Bethesda, Maryland) was used to determine the area of new fibrocartilage formation by manually outlining the area of metachromasia on the safranin O slides. The total area of metachromasia was then recorded in mm^2 for each sample.[36]

Semi quantitative analysis of collagen deposition and maturation at the repair site was

performed on the tissue sections stained with picrosirius red. Measurements were obtained by rotating the polarization plane until maximum brightness. By quantifying the collagen birefringence under polarized light, differences in collagen maturity and organization in the healing tendon could be detected. After a photomicrograph was captured, the image was imported into Image J; the image underwent 8-bit digitization, producing an image in which noncollagenous material was dark (zero) and collagenous material was in grayscale with values from 1 to 255.[29] Ten square areas (50 μm × 50 μm) were randomly selected from the tendon region adjacent to the insertion site.

2.5.3 Biomechanical evaluations

At 2, 4 and 8 weeks after surgery, 24 animals were sacrificed for biomechanical testing (8 rats per group per time point). The humerus with attached supraspinatus tendon was dissected from the surrounding tissues. The cross-sectional area of each supraspinatus tendon at the insertion site was measured using a digital caliper. The specimen was then placed into a custom-designed uniaxial testing system onto which the tendon and the humerus were secured firmly. The specimen was preloaded to 0.1 N and then loaded to failure at a rate of 14 μm/s, corresponding to about 0.4% strain. The linear region of the stress-strain curve was used to determine the stiffness for each specimen. Ultimate stress at failure was calculated by dividing the ultimate load to failure by the cross-sectional area of the specimen.[36-38]

2.6 Data Analysis

Approval for this study was obtained from the University Animal Care Committee of Shanghai Jiao Tong University. All authors were blinded to which study group or time interval the specimens belonged to at the time of microCT, histomorphometric analysis and biomechanical testing.

All data were presented as the mean ± SD. Statistical analysis was performed using

one-way analysis of variance with post hoc testing using the Holm-Sidak method. Significance was set at $p<0.05$.

3. Results

3.1 Morphology of stagger-electrospun fibrous scaffolds

In this work, homogeneous single or dual-scale fibrous scaffold of PCL microfibers alone or along with CS nanofibers were prepared. The electrospun PCL and stagger-electrospun PCL-CS fibers were both found to be uniform in size, forming randomly interconnected structures (see example in Figure 1 a and b). For the PCL-CS scaffolds, CS nanofibers were well distributed and integrated with the PCL microfibers throughout the entire scaffolds (see example in Figure 1b). The fiber diameter distribution of PCL showed a single peak around 1.2 ± 0.3 μm (Figure 1c). The fiber diameter distribution of PCL-CS showed two peaks at 1.2 ± 0.3 μm (PCL fibers) and 360 ± 23 nm (CS fibers) (Figure 1d). Calculated scaffold porosity was 70 ± 6% and 74 ± 5% for electrospun PCL and PCL-CS fibrous scaffolds, respectively, and there was no significant difference in the porosity between the two samples ($p >$ 0.05).

3.2 Mechanical properties of the electrospun fibrous scaffolds

Examination of the tensile properties of the material revealed that the tensile strength of stagger-electrospun PCL-CS scaffolds was 2.78 ± 0.3 MPa, comparable with that of PCL, 2.89 ± 0.3 MPa and approximately two times as high as that of CS scaffolds, 1.47 ± 0.2 MPa. The failure strain (elongation at break) of stagger-electrospun PCL-CS scaffolds was 405 ± 40%, slightly lower than that of PCL scaffolds, 470 ± 50%, but much higher than that of CS, 5.5 ± 1% (see example in Figure. 2 a and b). The tensile modulus of stagger-electrospun PCL-CS was found to be 26.2 ± 2.9 MPa, between that of PCL scaffolds, 17.8 ± 2.0 MPa and CS scaffolds, 39.1 ± 4.2 MPa. The improved strength and failure strain of PCL-CS scaffolds compared to that of CS scaffolds and enhanced stiffness compared to PCL scaffolds have suggested that the

PCL-CS scaffolds exhibited properties of both tendon (withstanding tension) and bone (resisting force).

Finite element analysis of the elastic region of the PCL and PCL-CS scaffolds have shown a single node force of 0.237 N and a total pull of the left and right-sided force of 4.74 N for PCL scaffolds and an increased single node force of 0.348 N and a total pull of the left and right-sided force of 6.96 N for PCL-CS scaffolds (Figure 2 c and d). These results have suggested that larger amount of force may be needed for the PCL-CS scaffolds to obtain the same strain as PCL scaffolds under stress and PCL-CS may have better capability to dissipate energy (minimize stress concentration, compare Figure 2 c and d) compared to PCL alone. This also explained the increase in the stiffness of the PCL-CS scaffolds while maintaining the strength and failure strain.

The cyclic curves of the electrospun PCL and PCL-CS fibrous scaffolds under a strain of 5% were shown in Figure 2 e and f, respectively. It was found that the electrospun fibrous scaffolds, either PLC or PCL-CS could recover their original shape after repeated 50 cycles.

3.3 Surface wettability, water sorption and degradation properties of the electrospun fibrous scaffolds

As shown in Figure 3 a, the WCAs of PCL-CS scaffolds decreased from average 121.6° to average 40.3° after 10 min whereas that of the PCL scaffolds kept constant around 133.0° after 10 min. The decreased WCAs of PCL-CS scaffolds (indicating increased surface wettability) may be beneficial for cell attachment and proliferation (as indicated by later *in vitro* cell proliferation results) as hydrophilic polymers usually exhibit better cell attachment and proliferation compared to hydrophobic polymers.[39]

As demonstrated in Figure 3 b-d, incorporation of CS nanofibers have resulted in

increased water absorption, faster reduction of molecular weight (Mw) of PCL and accelerated mass loss of the fibrous matrix. It was found that the water sorption of the PCL-CS scaffolds increased by about 2.9 times compared to that of PCL scaffolds (Figure 3 b). There was 9.7% and 41.9% of PCL Mw loss for PCL and PCL-CS fibrous scaffolds after incubation in PBS for 14 weeks, respectively (Figure 3c). The mass loss for PCL and PCL-CS fibrous scaffolds after incubation for 14 weeks were found to be 23.5% and 58.4%, respectively (Figure 3e). The more rapid degradation may be advantageous to allow better tissue regeneration.

3.4 Cell proliferation on the electrospun scaffolds

Cell morphology was examined using SEM after culture on electrospun PCL and PCL-CS scaffolds after 1, 3 and 7 days. Cells displayed fibroblastic morphology on both scaffolds whereas cells on PCL-CS scaffolds seemed to have better cell attachment (see example in Figure 4 a and b). Quantification of cell proliferation on PCL and PCL-CS scaffolds using MTT assay has shown significantly increased cell proliferation on PCL-CS scaffolds compared to PCL scaffolds (Figure 4c). In particular, cell proliferation on PCL-CS scaffolds after 7 days of culture was approximately two times higher than that of PCL scaffolds.

3.5 Tissue regeneration using electrospun scaffolds

The RCT of rats healed properly with no apparent appearance of infection at the surgical site in any of the specimens after implantation. The repaired tendon was attached to the bone in all animals. The shoulders in both experimental groups had residual scaffolds present around the insertion site at 2 weeks after surgery. After 4 weeks of implantation, PCL-CS scaffolds disappeared whereas PCL scaffolds remained. After 8 weeks of surgery, no scaffolds were observed at any surgical site.

3.5.1 Microcomputed tomography analysis

Reconstructed microCT images of the proximal humerus were used to demonstrate

the morphologies of the regenerated bone (see example in Figure 5 A). The tendon-bone insertion site of the proximal humerus after implantation with stagger-electrospun PCL-CS scaffolds showed more significant bone formation compared to that with no implant and with the electrospun PCL.

MicroCT analysis showed that the tissues repaired using the PCL-CS group showed significant increase in BMD, TMD and BV/TV at all times compared to those repaired with no scaffolds or with PCL scaffolds (Figure 5B). There was no significant difference in BMD, TMD and BV/TV between the control and the PCL group. These results have suggested that the PCL-CS fibrous scaffolds exhibited a remarkable capacity to enhance new bone formation at the tendon-bone interface, with potentially increased RCT healing success rate. This finding corresponded well with previous reports which observed that CS-incorporated fibrous scaffolds favoured osteogenesis[40,41] owing to the good osteoconductive property of CS.[42]

3.5.2 Cellularity and host tissue response analysis

After 2 weeks of surgery, both PCL and PCL-CS scaffolds were present at the surgery site (Figure 6). Spindle-shaped cells were observed at the interstices of the scaffold fibers regardless of PCL or PCL-CS scaffolds. At 4 weeks, PCL scaffolds could still be observed whereas PCL-CS scaffolds disappeared. For both PCL and PCL-CS scaffolds, fibroblasts aligned irregularly with moderate cellularity and vascular formation at the repaired site. At 8 weeks, no scaffolds , PCL or PCL-CS, were present in any sample. Cells aligned regularly with decreased cellularity. The insertion site of the PCL-CS group contained the greatest number of paralleled fibrous tissues in the fibrocartilage.

3.5.3 Metachromasia analysis

With increased time after surgery, all three groups (control, PCL and PCL-CS) showed increased area of glycosaminoglycan staining indicating presence of cartilage

at the tendon-bone interface. The PCL-CS group displayed greatest total area of metachromasia (suggesting cartilage formation), followed by the PCL group and then the control group at all three time points (Figure 7). The results have suggested that PCL, especially PCL-CS scaffolds, exhibited the capacity to improve cartilage regeneration at the tendon-bone interface.

3.5.4 Collagen organization analysis

Picro-Sirius red staining was used in the histological visualization of collagen I and III fibers in tissue sections. At 2 weeks after surgery, PCL and PCL-CS scaffolds had significantly improved collagen organization based on birefringence under polarized light at the healing enthesis compared with the control group (18.5 ± 0.6 gray-scale units for controls, 20.6 ± 1.1 for PCL, and 22.5 ± 0.8 for PCL-CS) (Figure 8). The collagen birefringence for the PCL-CS group was significantly greater in comparison with the PCL group. At 4 and 8 weeks after surgery, experimental groups had significantly improved collagen organization based on the birefringence compared with the control group (29.8 ± 0.9 and 42.0 ± 1.4 gray-scale units for controls, 31.7 ± 0.9 and 43.8 ± 1.0 for PCL, 32.2 ± 1.1 and 44.8 ± 1.1 for PCL-CS). These results have demonstrated that the PCL-CS group had improved collagen production compared to the other groups, especially at the early stage. For the PCL-CS group, comparing the 4 week and 8 week result, the collagen birefringence for the PCL-CS group at 8 weeks after surgery was significantly greater in comparison with that at 4 weeks with improved collagen organization. The resultant increased mineral content and collagen production due to implantation of PCL-CS scaffolds are critical for functional and integrative tendon repair.[43]

3.6 Mechanical properties of healing enthesis

In general, the cross-sectional area of the healing enthesis repaired using PCL or PCL-CS scaffolds were larger compared to the control group with no implantation, particularly at later time points (Figure 9A). The ultimate load to failure, stiffness and

ultimate stress of the repaired supraspinatus tendon–bone construct increased with time regardless with methods of repair. The supraspinatus tendon-bone construct repaired using PCL-CS scaffolds had significant higher ultimate load to failure, stiffness and ultimate stress than that repaired using PCL scaffolds or self-healing, particularly at later time points (Figure 9 B-D). These results have indicated that the mechanical strength of the supraspinatus tendon–bone construct augmented successfully with PCL-CS scaffolds.

4. Discussion

In this study, a homogeneous dual scaffolding system composed of PCL microfibers and interspersed CS nanofibers was prepared using stagger-electrospinning strategy. Unlike traditional blending electrospinning (electrospinning a mixture of polymer solution through a single spinneret), the stagger-electrospinning strategy has the advantage of controlling scaffold chemical composition through the use of polymers with different chemical and physical properties that can be selectively incorporated. The different polymeric components maintain their individual properties, and contribute to the overall properties of the scaffold in a tailored and controlled way.[23] In this specific study, the dual scaffolding system has PCL microfibers to make it stretchable and CS nanofibers to make it stiff and biocompatible. Moreover, the dual fiber size of the scaffolds further endows the scaffolds with additional advantages with microfibers to improve its mechanical properties and nanofibers to aid tissue regeneration.

The plain CS scaffold after crosslinking was highly rigid and brittle as a consequence of cross-junction between macromolecular chains, whereas the PCL scaffold showed a lower tensile modulus and higher elongation at break with respect to CS. It has been previously demonstrated that combination, through stagger-electrospinning, of two individual fiber components with dissimilar mechanical properties has an influence on the mechanics of the composite scaffold which displays properties of both fiber

components.[44-46] Indeed, the knitted dual PCL-CS scaffolding system combines the advantages of individual polymers. The dual PCL-CS scaffolding system (strength 2.8 MPa, failure stain ~ 400% and stiffness ~26 MPa) demonstrated an increased strength and failure strain like PCL (strength ~2.9 MPa, failure strain ~470% and stiffness ~18 MPa) as well as enhanced stiffness like CS (stiffness ~39 MPa, strength ~1.5 MPa, failure strain ~5%). The increased strength and strain indicates improved capability to withstand tension (properties of tendon) while the enhanced stiffness suggests better ability to resist force (properties of one). The knitted dual PCL-CS scaffolding system has more comparable mechanical properties to the tendon-bone compared to the PCL or CS scaffolds, making the scaffold more appropriate for augmentation of RCT healing.

In addition, it was found that the dual PCL-CS scaffolding system has increased surface wettability, improved cell attachment and proliferation, raised water sorption and accelerated degradation rate compared to the single PCL scaffold system. The electrospun PCL scaffolds were hydrophobic, on which cell adhesion was poor *in vitro*. It did not promote cell proliferation at the early stage. Incorporation of hydrophilic CS nanofibers resulted in increased surface wettability and cell attachment and proliferation and more rapid degradation of the scaffolds. The fast degradation may be beneficial to promote subsequent bone and cartilage regeneration.

Furthermore, treatment usign stagger-electrospun PCL-CS fibrous scaffolds promoted new bone and fibrocartilage formation, improved collagen organization, and strengthened the healing enthesis compared to PCL alone in a chronic RCT model, with no presence of inflammatory response, as suggested by the radiological, histological and biomechanical investigations. This improvement may be due to the nanofeatures of CS nanofibers which more closely resemble native structures of the ECM, thus leading to better cell proliferation, ECM deposition and tissue regeneration.[21,22]

Our study represents the first implementation of stagger-electrospun hierarchical scaffolding system of dual scale fibers which is both stretchable and stiff for augmentation of RCT repair. These dual scaffolding sytems almost meet the physiologic requirements of the native tendon-bone tissues by matching its mechanical properties while simultaneously promoting tissue regeneration by mimicking the ultrastructural organization of the native tissue. These scaffolds are gradually degraded and replaced by new tissue with comparable structures to the original tissues. Moreover, the scaffolds exhibit integration with the host tendon and surrounding bone tissue by promoting the bone mineralization and ECM deposition which are critical parameters for functional and integrative tendon-bone tissue repair.[43-46] The superior mechanical and biological properties of the hierarchical, stretchable and stiff fibrous scaffolds demonstrated meaningful breakthrough by the combination therapy of stagger-electrospun nanoscale CS and microscale PCL fibers in chronic RCT repair.

5. Conclusion

Hierarchical, stretchable and stiff fibrous scaffolds of micro- and nano- fibrous scaffolds were successfully fabricated using a stagger-electrospinning process. These scaffolds exhibited more comparable mechanical properties to the tendon-bone interface, which may be beneficial for augmentation of RCT healing. Local application of these scaffolds to the tendon-bone interface in a chronic RCT rat model was found to promote the new bone formation, ECM deposition and strengthen the healing enthesis. These hierarchical, stretchable and stiff fibrous scaffolds engineered using stagger-electrospinning may be a suitable candidate for augmentation of RCT-healing clinically.

Acknowledgments

This work was supported by the National Natural Science Foundation of China (51373112 and 31370945) and China Scholarship Council (CSC).

References

1. B. G. Domb, R. E. Glousman, A. Brooks, M. Hansen, T. Q. Lee and N. S. ElAttrache, *J. Bone Joint Surg. Am.*, 2008, **90**, Suppl 4:35-39.
2. C. O. Nelson, M. J. Sileo, M. G. Grossman and F. Serra-Hsu, *Arthroscopy*, 2008, **24**, 941-948.
3. S. L. Tocci, R. Z. Tashjian, E. Leventhal, D. B. Spenciner, A. Green and B. C. Fleming, *J. Shoulder Elb. Surg*., 2008, **17**, 808-814.
4. M. E. Angeline and S. A. Rodeo, *Clin. Sport. Med.,* 2012, **31**, 645-663.
5. C. Gerber, A. G. Schneeberger, S. M. Perren and R. W. Nyffeler, *J. Bone Joint Surg. Am*., 1999, **81**, 1281-1290.
6. S. A. Rodeo, H. G. Potter, S. Kawamura, A. S. Turner, H. J. Kim and B. L. Atkinson, *J. Bone Joint Surg. Am*., 2007, **89**, 2485-2497.
7. S. Yamazaki, K. Yasuda, F. Tomita, H. Tohyama and A. Minami, *Arthroscopy*, 2005, *21*, 1034-1041.
8. A. K. Chong, A. D. Ang, J. C. Goh, J. H. Hui, A. Y. Lim, E. H. Lee and B. H. Lim, *J Bone Joint Surg. Am.,* 2007, **89**, 74-81.
9. L. Qin, H. Lu, P. Fok, W. Cheung, Y. Zheng, K. Lee and K. Leung, *Ultrasound Med. Bio*l., 2006, **32**, 1905-1911.
10. D. Kovacevic and S. A. Rodeo, *Clin. Orthop. Relat. R.,* 2008, **466**, 622-633.
11. M. Ozbaydar, B. Elhassan, C. Esenyel, A. Atalar, E. Bozdag, E. Sunbuloglu, N. Kopuz and M. Demirhan, *J Bone Joint Surg. Br*., 2008, **90**, 1386-1391.
12. M. F. Pietschmann, V. Froehlich, A. Ficklscherer, B. Wegener, V. Jansson and P. E.Muller, *J. Shoulder Elb. Surg*., 2008, **17**, 642-646.
13. T. A. Wren, S. A. Yerby, G. S. Beaupre and D. R. Carter, *Clin. Biomech*., 2001, **16**,245-251.
14. M. R. Ladd, S. J. Lee, J. D. Stitzel, A. Atala and J. J. Yoo, *Biomaterials*, 2011, **32**,1549-1559.
15. K. Tuzlakoglu, N. Bolgen, A.J. Salgado, M.E. Gomes, E. Piskin and R. L. Reis. *J. Mater. Sci.-Mater. M.*, 2005, **16**, 1099-1104.

16. Q. P. Pham, U. Sharma and A.G. Mikos. *Biomacromolecules*. 2006, **7**, 2796-2805.
17. S. Soliman, S. Pagliari, A. Rinaldi, G. Forte, R. Fiaccavento, F. PagliariF, O. Franzese, M. Minieri, P. Di Nardo, S. Licoccia and E. Traversa. *Acta Biomater*. 2010, **6**, 1227-1237.
18. S.H. Park, T.G. Kim, H.C. Kim, D.Y. Yang and T.G. Park. *Acta Biomater*., 2008, **4**, 1198-1207.
19. K.L. Moffat, A.S. Kwei, J.P. Spalazzi, S.B. Doty, W.N. Levine and H.H. Lu. *Tissue Eng. Pt. A,* 2009, **15**, 115-126.
20. A. Inui, T. Kokubu, H. Fujioka, I. Nagura, R. Sakata, H. Nishimoto, M. Kotera, T.Nishino and M. Kurosaka, *Sports Med. Arthrosc. Rehabil. Ther. Technol*., 2011, **3**, 29.
21. J. Xie, X. Li, J. Lipner, C. N. Manning, A. G. Schwartz, S. Thomopoulos and Y. Xia, *Nanoscale*, 2010, **2**, 923-936.
22. Y. Zhu, C. Hu, B. Li, H. Yang, Y. Cheng and W. Cui, *Acta Biomater*., 2013, **9**, 8328-8336.
23. S. Sahoo, J. G. Cho-Hong and T. Siew-Lok, *Biomed. Mater*., 2007, **2**, 169-173.
24. Y. Zhang, J. R. Venugopal, A. El-Turki, S. Ramakrishna, B. Su and C. T. Lim, *Biomaterials*, 2008, **29**, 4314-4322.
25. N. Bhattarai, D. Edmondson, O. Veiseh, F. A. Matsen and M. Zhang, *Biomaterials*, 2005**, 26**, 6176-6184.
26. C. Hu and W. Cui, *Adv. Healthc. Mater*., 2012, **1**, 809-814.
27. W. Cui, Y. Zhou and J. Chang, *Sci. Technol. Adv. Mat*., 2010, **11**, 014108.
28. P. Torricelli, M. Gioffre, A. Fiorani, S. Panzavolta, C. Gualandi, M. Fini, M. L. Forcarete and A. Bigi, *Mater. Sci. Eng. C Mater. Biol. Appl*., 2014, **36**, 130-138.
29. W. Cui, L. Cheng, H. Li, Y. Zhou and Y. Zhang, *Polymer,* 2012, **53**, 2298-2305.
30. M. Prabaharan and J. F. Mano, *Macromol. Biosci*., 2006, **6**, 991-1008.
31. J. Pu, X. J. Yan, Y. D. Jiang, C. Chang and L. W. Lin, *Sensor. Actuator. A-Phys.*, 2010, **164**, 131–136.

32. S. Buchmann, L. Walz, G. H. Sandmann, H. Hoppe, K. Beitzel, G. Wexel, A. Battmann, S. Vogt, S. Hinterwimmer and A. B. Imhoff, *Arch. Orthop. Traum. Su.*, 2011, **131**, 429-435.
33. S. Thomopoulos, G. Hattersley, V. Rosen, M. Mertens, L. Galatz, G. R. Williams and L. J. Soslowsky, *J. Orthop. Res*., 2002, **20**, 454-463.
34. R.H. Brophy, D. Kovacevic, C.W. Imhauser, M. Stasiak, A. Bedi, A.J. Fox, X.H. Deng and S.A. Rodeo. *J. Bone Joint Surg. AM*., 2011, **93**, 381-393.
35. J.D. Packer, A. Bedi, A.J. Fox, S. Gasinu, C.W. Imhauser, M. Stasiak, X.H. Deng and S.A. Rodeo. *J. Bone Joint Surg. AM*., 2014, **96**, 770-777.
36. D. Kovacevic, A. J. Fox, A. Bedi, L. Ying, X. H. Deng, R. F. Warren and S. A. Rodeo, *Am. J. Sports Med.,* 2011, **39**, 811-819.
37. A. Bedi, A. J. Fox, D. Kovacevic, X. H. Deng, R. F. Warren and S. A. Rodeo, *Am. J. Sports Med*., 2010, **38**, 308-317.
38. L. V. Gulotta, D. Kovacevic, S. Montgomery, J. R. Ehteshami, J. D. Packer and S.A. Rodeo, *Am. J. Sports Med.*, 2010, **38**, 1429-1437.
39. D. P. Dowling, I. S. Miller, M. Ardhaoui and W. M. Gallagher, *J. Biomater. Appl*.,2011, **26**, 327-347.
40. S.Y. Shin, H.N. Park, K.H. Kim, M.H. Lee, Y.S. Choi, Y.J. Park, Y.M. Lee, Y. Ku, I.C. Rhyu, S.B. Han, S.J. Lee and C.P. Chung. *J. Periodontol.* 2005, **76**, 1778-1784.
41. G. Toskas, C. Cherif, R.D. Hund, E. Laourine, B. Mahltig, A. Fahmi, C. Heinemann and T. Hanke. *Carbohydr. Polym*. 2013, **94**, 713-722.
42. M.N. Kumar, R.A. Muzzarelli, C. Muzzarelli, H. Sashiwa and A.J. Domb. *Chem. Rev*. 2004, **104**, 6017-6084.
43. X. Zhang, D. Bogdanowicz, C. Erisken, N. M. Lee and H. H. Lu, *J Shoulder Elb. Surg*. 2012, **21**, 266-277.
44. S. Samavedi, C. Olsen Horton, S. A. Guelcher, A. S. Goldstein and A. R. Whittington, *Acta Biomater*. 2011, **7**, 4131-4138.

45. Z. Chen, L. Cao, L. Wang, H. Zhu and H. Jiang, *J. Appl. Polym. Sci.*, 2013, **127**, 4225-4232.

46. N. Detta, C. Errico, D. Dinucci, D. Puppi, D. A. Clarke, G. C. Reilly and F. Chiellini, *J. Mater. Sci. Mater. Med*. 2010, **21**, 1761-1769.

Figures Captions

Scheme 1. Illustrations of fabrication of dual scaffolding system composed of PCL microfibers and interspersed CS nanofibers using a stagger-electrospinning process with a rotating metal mandrel for augmentation of RCT tendon-healing.

Fig. 1. SEM images of the electrospun single PCL (a) and dual PCL-CS (b) fibers, and the fiber diameter distribution of PCL(c) and PCL-CS scaffolds (d).

Fig. 2 Mechanical properties of electrospun PCL and PCL-CS scaffolds. a and b: Stress–strain curves by tensile test for electrospun PCL and PCL-CS scaffolds. c and d: Finite element analysis of the elastic region of the PCL and PCL-CS scaffolds. e and f: Cyclic curves at 5% stain of the electrospun PCL and PCL-CS scaffolds.

Fig. 3 Water contact angles with time (a), water absorption (b), molecular weight reduction with time (c) and mass retention with time (d) for electrospun PCL and stagger-electrospun PCL-CS fibrous scaffolds.

Fig. 4 SEM images of cell morphology on the electrospun PCL (a) and stagger-electrospun PCL-CS fibrous scaffolds after 7 days of culture. (c) Quantification of C3 cell proliferation on the electrospun fibrous scaffold (n=3). Control = tissue culture plastic. * $p < 0.05$ compared to the PCL group.

Fig. 5 A. Representative microcomputed tomography (microCT) images of the proximal humerus after implantation with no (control) and with electrospun PCL and stagger-electrospun PCL-CS scaffolds. The red arrow indicates the tendon-bone insertion site. B. MicroCT analysis of bone mineral density (BMD), tissue mineral density (TMD), as well as bone volume fraction (bone volume/total volume, BV/TV). The results are shown as mean ± SD. (* $p < 0.05$ vs. control; ▲$p < 0.05$ vs. PCL; n = 8 for each group).

Fig. 6 Representative Hematoxylin and Eosin stained tissue sections of the tendon insertion site at 2, 4 and 8 weeks postoperatively. The green arrow indicates degraded fibrous scaffold, the yellow triangle indicates fibroblasts, and the red circle indicates microvessels. Note the presence of paralleled fibrous tissues and absence of microvessles after 8 weeks at the implant site using PCL-CS scaffolds.

Fig. 7 Representative safranin O/fast green stained images of cartilage at the insertion site (A) and quantification of the area of cartilage (red) present at the insertion site (B). T=Tendon; I = implant; B = bone. Results are shown as mean ± SD. (* $p < 0.05$ vs. control; ▲$p < 0.05$ vs. PCL; n = 8 for each group).

Fig. 8 Representative picrosirius red–stained tissue sections of the healing enthesis (A) and quantification of collagen birefringence (B). B=bone; I=implant; T=tendon. Results are shown as mean ± SD. (* $p < 0.05$ vs. control; ▲$p < 0.05$ vs. PCL; n = 8 for each group).

Fig. 9 Cross-sectional area (A), ultimate loads to failure (B), stiffness (C) and ultimate stress to failure (D) of the tendon at the insertion site repaired using self-healing, PCL or PCL-CS scaffolds. Results are shown as mean ± SD. (* $p < 0.05$ vs. control; ▲$p < 0.05$ vs. PCL; n = 8 for each group).

Scheme 1 Illustrations of fabrication of dual scaffolding system composed of PCL microfibers and interspersed CS nanofibers using a stagger-electrospinning process with a rotating metal mandrel for augmentation of RCT tendon-healing.

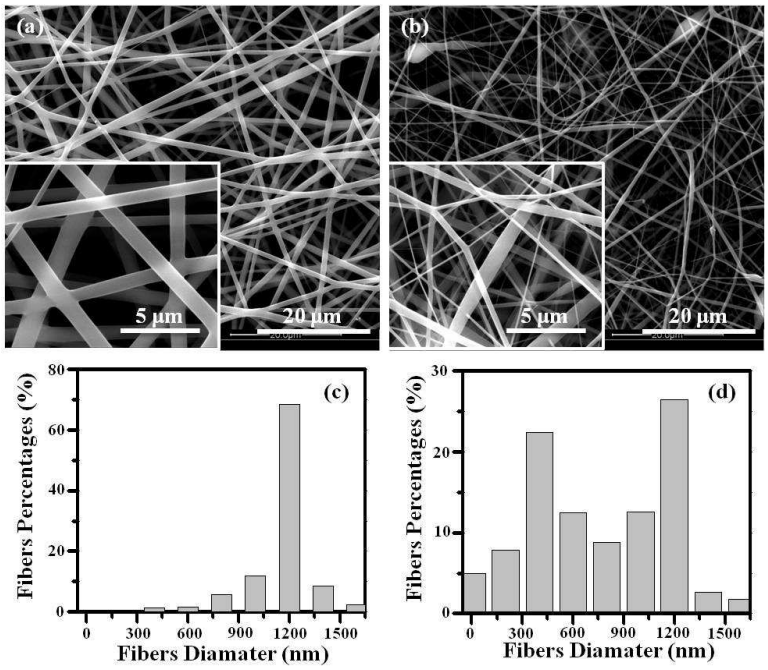

Fig. 1 SEM images of the electrospun single PCL (a) and dual PCL-CS (b) fibers, and the fiber diameter distribution of PCL(c) and PCL-CS scaffolds (d).

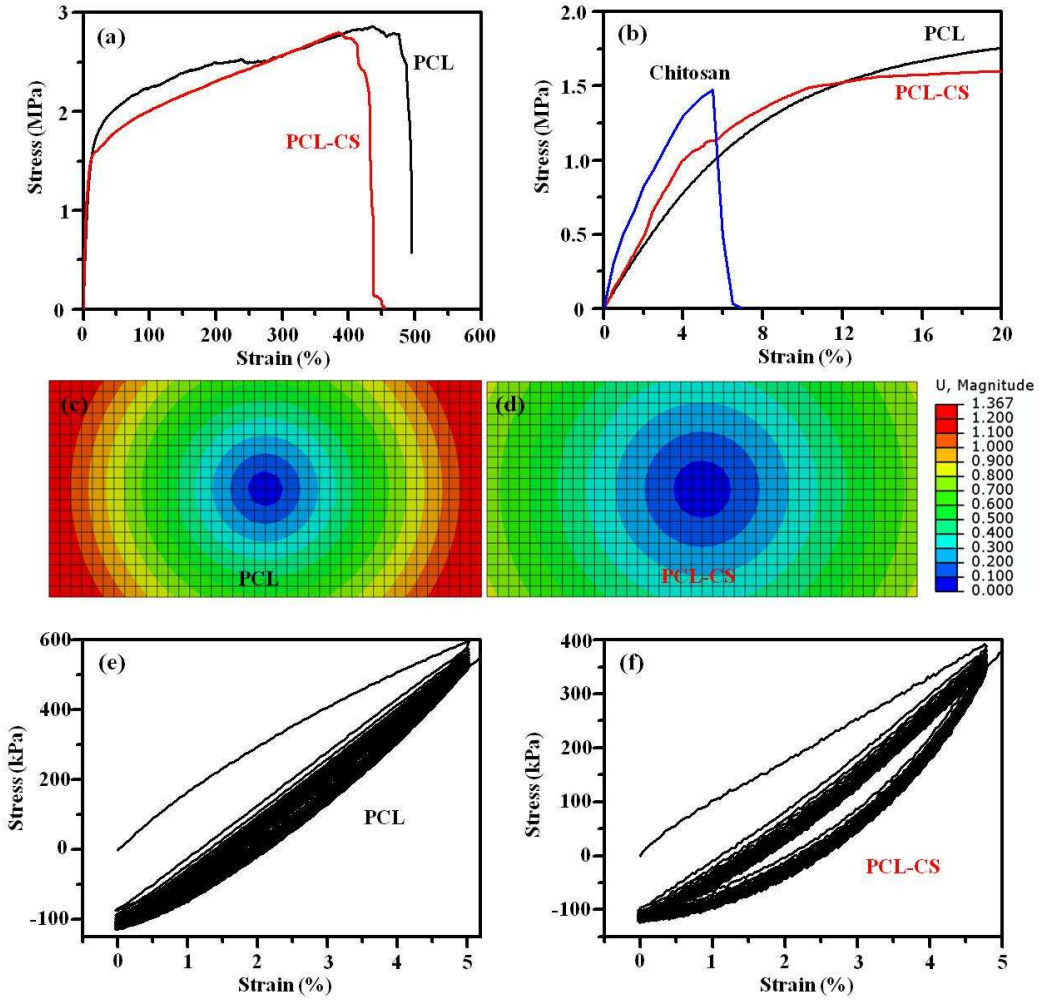

Fig. 2 Mechanical properties of electrospun PCL and PCL-CS scaffolds. a and b: Stress–strain curves by tensile test for electrospun PCL and PCL-CS scaffolds. c and d: Finite element analysis of the elastic region of the PCL and PCL-CS scaffolds. e and f: Cyclic curves at 5% stain of the electrospun PCL and PCL-CS scaffolds.

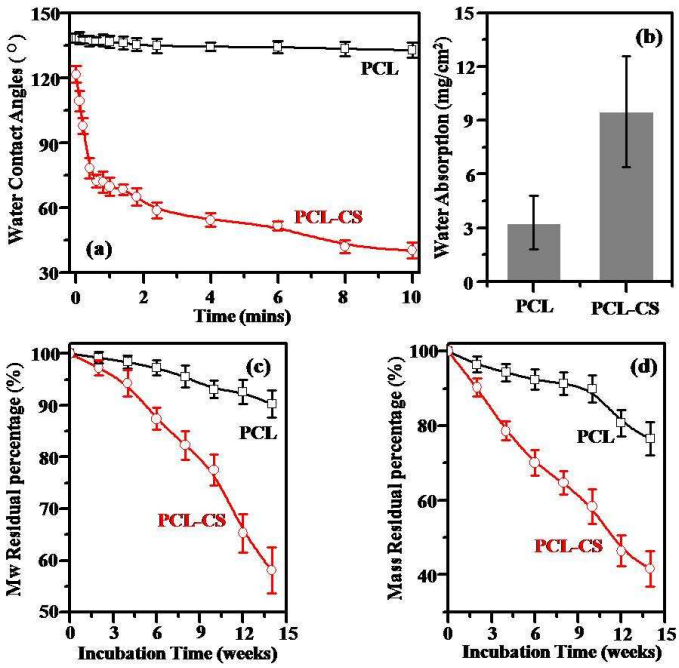

Fig. 3 Water contact angles with time (a), water absorption (b), molecular weight reduction with time (c) and mass retention with time (d) for electrospun PCL and stagger-electrospun PCL-CS fibrous scaffolds.

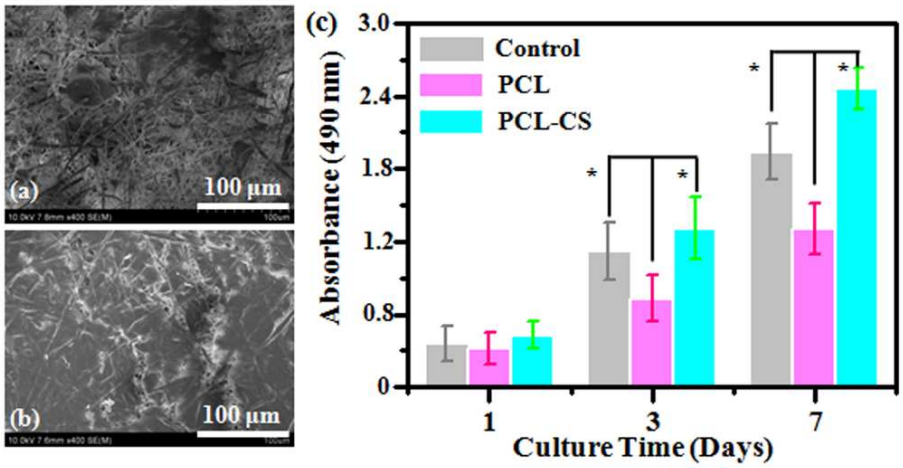

Fig. 4 SEM images of cell morphology on the electrospun PCL (a) and stagger-electrospun PCL-CS fibrous scaffolds after 7 days of culture. (c) Quantification of C3 cell proliferation on the electrospun fibrous scaffold (n=3). Control = tissue culture plastic. * $p < 0.05$ compared to the PCL group.

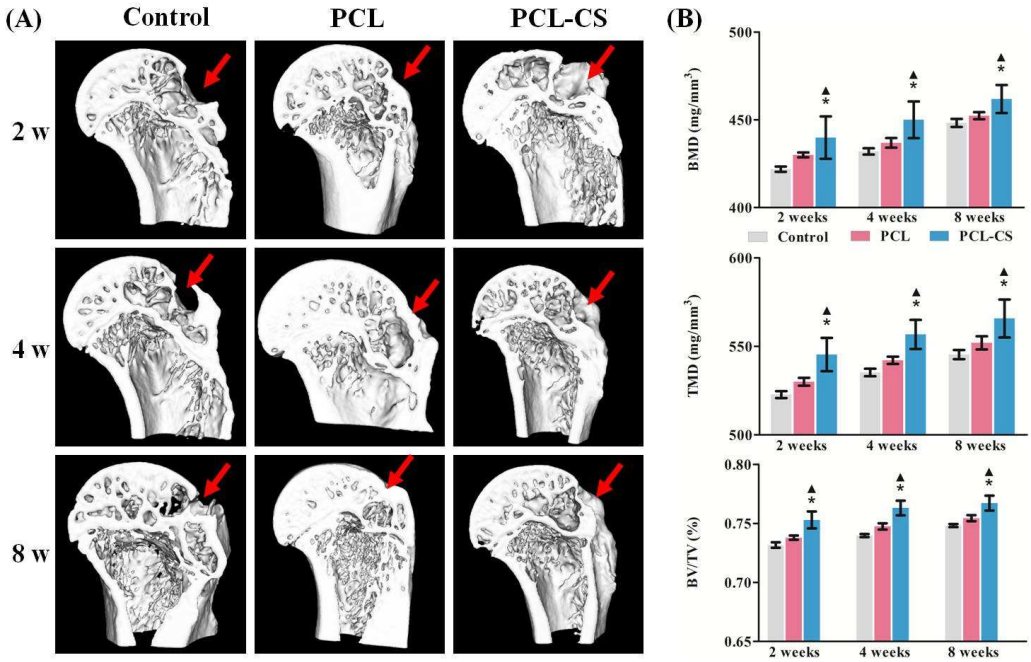

Fig. 5 A. Representative microcomputed tomography (microCT) images of the proximal humerus after implantation with no (control) and with electrospun PCL and stagger-electrospun PCL-CS scaffolds. The red arrow indicates the tendon-bone insertion site. B. MicroCT analysis of bone mineral density (BMD), tissue mineral density (TMD), as well as bone volume fraction (bone volume/total volume, BV/TV). The results are shown as mean ± SD. (* $p < 0.05$ vs. control; ▲$p < 0.05$ vs. PCL; n = 8 for each group).

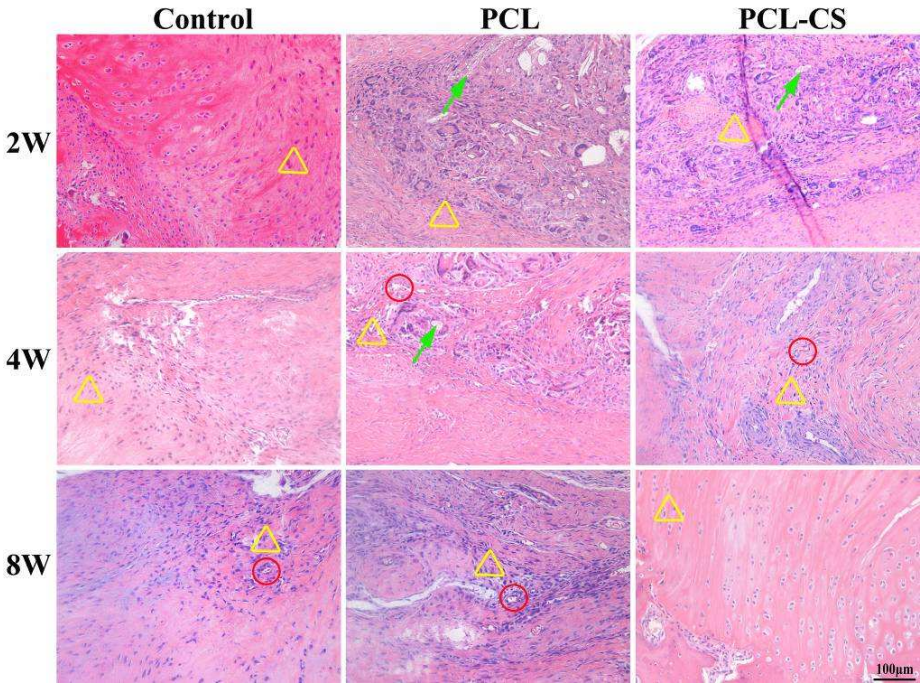

Fig. 6 Representative Hematoxylin and Eosin stained tissue sections of the tendon insertion site at 2, 4 and 8 weeks postoperatively. The green arrow indicates degraded fibrous scaffold, the yellow triangle indicates fibroblasts, and the red circle indicates microvessels. Note the presence of paralleled fibrous tissues and absence of microvessles after 8 weeks at the implant site using PCL-CS scaffolds.

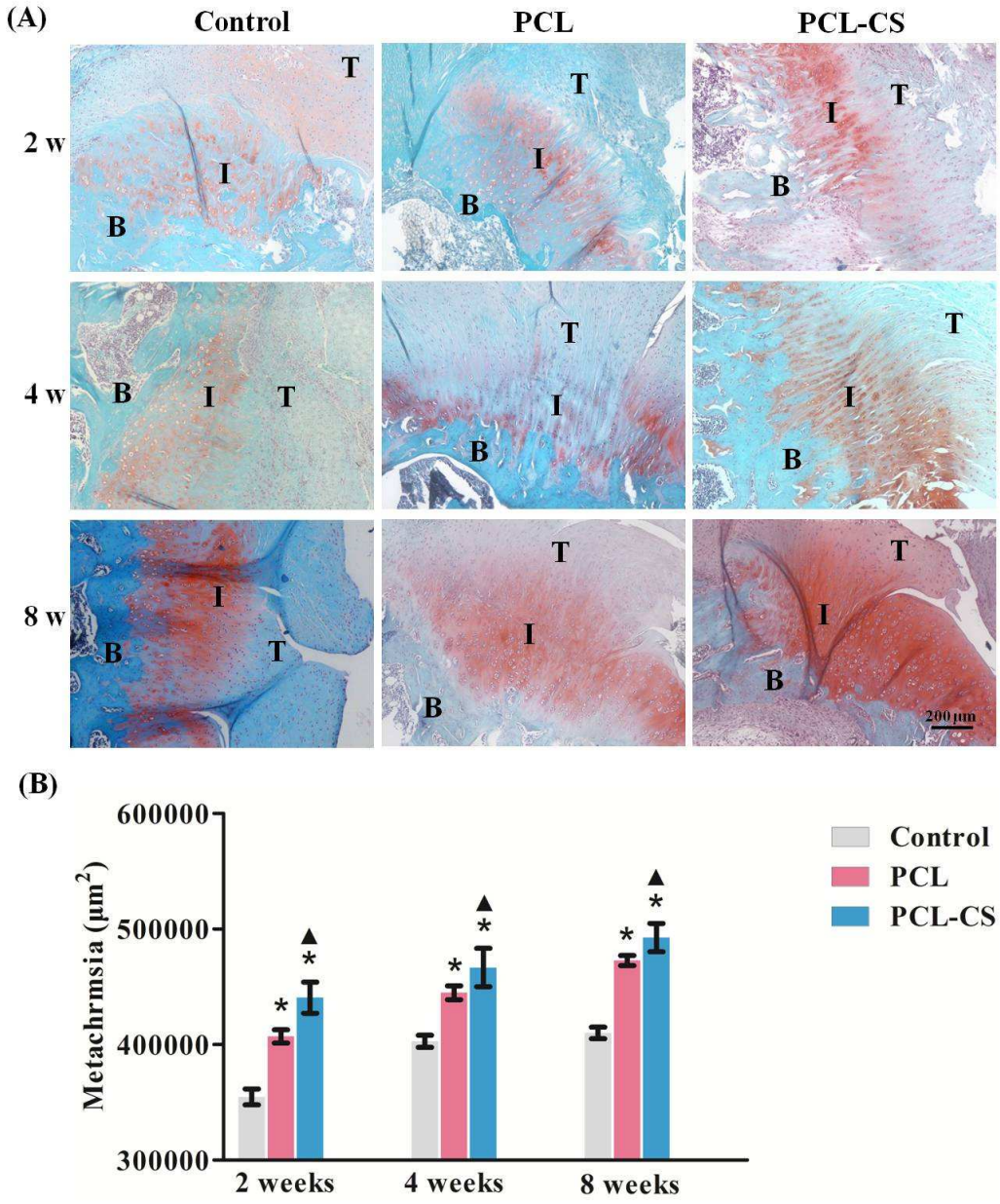

Fig. 7 Representative safranin O/fast green stained images of cartilage at the insertion site (A) and quantification of the area of cartilage (red) present at the insertion site (B). T=Tendon; I = implant; B = bone. Results are shown as mean ± SD. (* $p < 0.05$ vs. control; ▲$p < 0.05$ vs. PCL; n = 8 for each group).

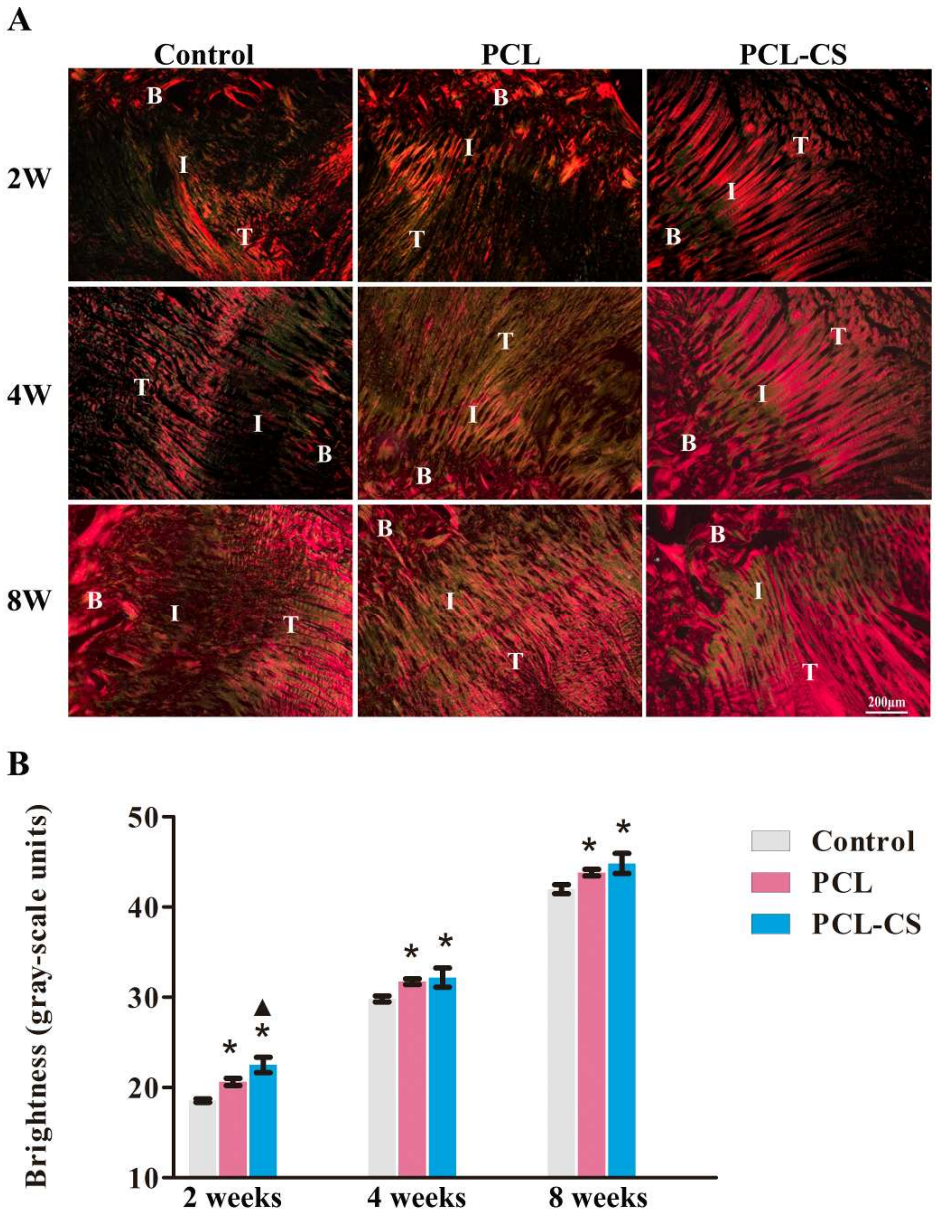

Fig. 8 Representative picrosirius red–stained tissue sections of the healing enthesis (A) and quantification of collagen birefringence (B). B=bone; I=implant; T=tendon. Results are shown as mean ± SD. (* $p < 0.05$ vs. control; ▲$p < 0.05$ vs. PCL; n = 8 for each group).

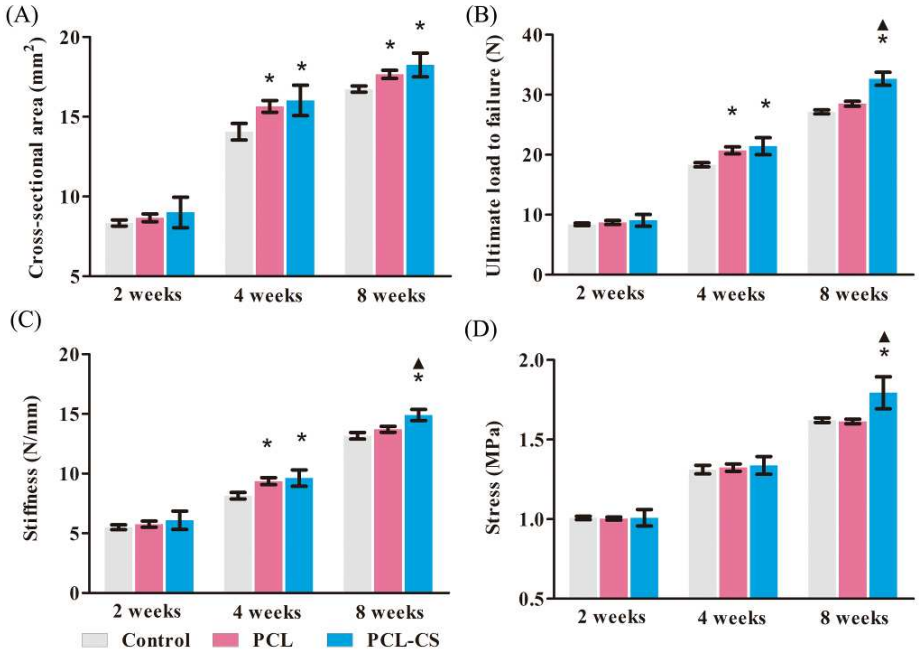

Fig. 9 Cross-sectional area (A), ultimate loads to failure (B), stiffness (C) and ultimate stress to failure (D) of the tendon at the insertion site repaired using self-healing, PCL or PCL-CS scaffolds. Results are shown as mean ± SD. (* $p < 0.05$ vs. control; ▲$p < 0.05$ vs. PCL; $n = 8$ for each group).

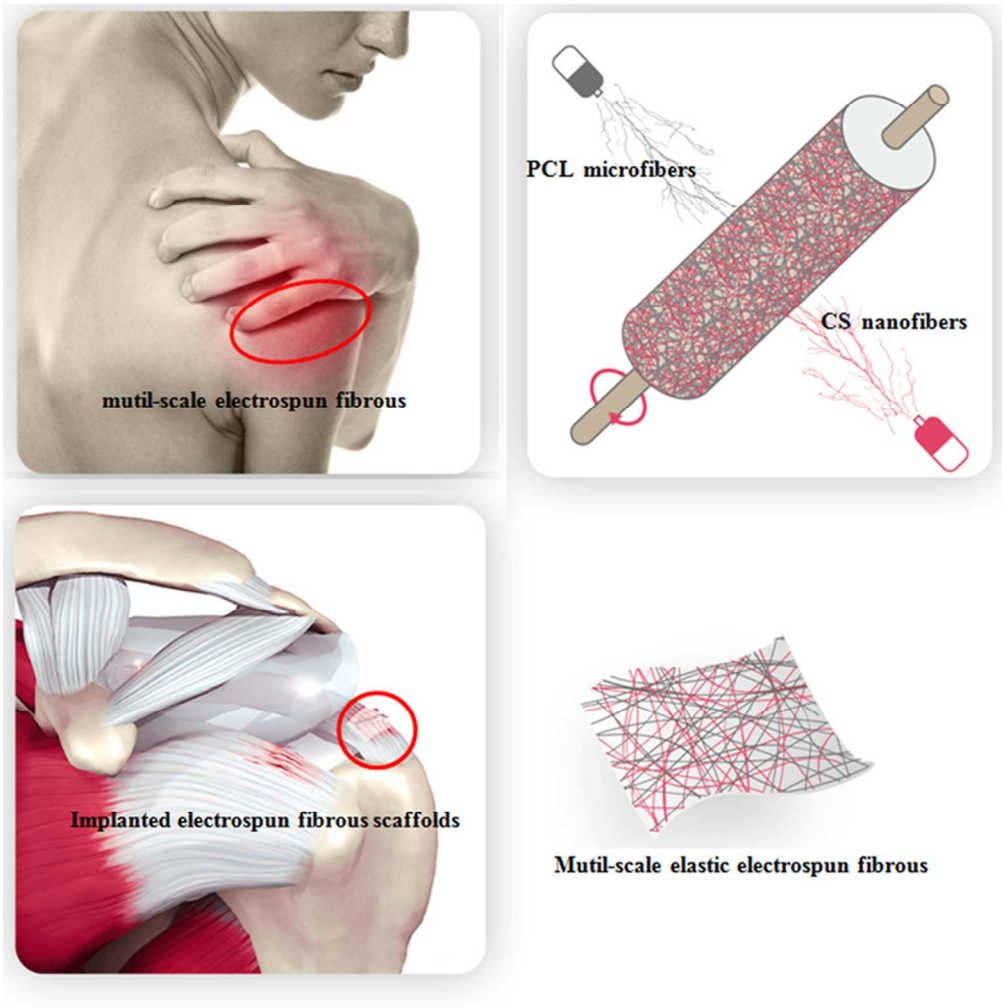

Engineering hierarchical, stretchable and stiff fibrous biotemplate using stagger-electrospinning for augmentation of rotator cuff tendon-healing
80x81mm (300 x 300 DPI)